International Journal of Solids and Structures 110–111 (2017) 305–314

Contents lists available at ScienceDirect

International Journal of Solids and Structures

journal homepage: www.elsevier.com/locate/ijsolstr

Shear deformation dominates in the soft adhesive layers of the laminated structure of flexible electronics

Shuang Li[a], Xiaoli Liu[b], Rui Li[c,*], Yewang Su[a,c,d,*]

[a] State Key Laboratory of Nonlinear Mechanics, Institute of Mechanics, Chinese Academy of Sciences, Beijing 100190, China
[b] State Key Laboratory of Hydroscience and Engineering, Tsinghua University, Beijing 100084, China
[c] State Key Laboratory of Structural Analysis for Industrial Equipment, Department of Engineering Mechanics, Dalian University of Technology, Dalian 116024, China
[d] School of Engineering Science, University of Chinese Academy of Sciences, Beijing 100049, China

ARTICLE INFO

Article history:
Received 17 July 2016
Revised 24 November 2016
Available online 9 December 2016

Keywords:
Shear deformation
Adhesive layer
Laminated structure
Flexible electronics

ABSTRACT

Flexible electronics has attracted much attention in recent years due to the favorable applications to many emerging devices. A novel laminated structure for a new-generation of flexible electronics is composed of several thin layers, where the hard functional components are built, glued by soft adhesives. To prevent the premature mechanical failure and to achieve the best performance of the electronics, the structural design of such a laminate is of crucial importance. Accordingly, it is necessary to establish an analytic model to accurately describe the mechanical behavior of the laminated structure. The available models fall into two categories: those only taking into account the normal strain-induced deformation of the soft adhesive layers and those only incorporating the shear deformation of the same layers. This paper aims to quantitatively figure out which deformation dominates. By establishing an accurate enough analytic model, a significant finding is revealed that shear deformation dominates in the soft adhesive layers of the laminated structure of flexible electronics while the normal strain-induced deformation is negligible. The model is well validated by the finite element method (FEM). The effects of the membrane energy and bending energy of the soft layer are also investigated by incorporating or neglecting the shear energy. The model accurately captures the key quantities such as the strain distribution in each layer and the locations of the neutral mechanical planes of the top and bottom layers. This work is expected to provide the design guidelines for the laminated structure-based flexible electronics.

1. Introduction

Flexible electronics are receiving extensive attention for their combining the excellent electric performance with attractive flexibility of the electronics. Due to the favorable properties, many emerging flexible electronic applications and their variants with the stretchability have been developed such as stretchable and foldable silicon integrated circuits (Kim et al., 2008; Li et al., 2013b), electronic eye cameras (Ko et al., 2008; Song et al., 2013), epidermal electronics (Kim et al., 2011), fingertip electronics (Su et al., 2013; Ying et al., 2012), transient electronics (Hwang et al., 2012; Li et al., 2013a), stretchable batteries (Xu et al., 2013) and conformal piezoelectric energy harvesters (Dagdeviren et al., 2014; Su et al., 2015a).

Laminated structures were first used in mechanical and civil engineering, and have been widely employed for many years, of which the most popular ones are lightweight sandwich panels, with two hard face sheets separated by a soft foam core (Allen, 1969; Hohe et al., 2006; Li and Kardomateas, 2008; Zhu et al., 2008). Such structures have excellent mechanical properties such as high rigidity, high impact energy absorption, stable deformation mode and adaptation to loading conditions. Similar design has recently been applied to a class of novel flexible electronics by stacking several hard layers, with the soft layers in between (Kim et al., 2012; Kim et al., 2010; Rogers et al., 2010). The hard layers serve as the functional components of a device, and the soft layers are adhesives. As shown in Fig. 1(a), three thin PZT-based piezoelectric layers are laminated to achieve a conformable piezoelectric mechanical energy harvester (Li et al., 2016; Su et al., 2015b). This design is actually inspired by that used for flexible glass photonic devices (Li et al., 2014), of which a flexible photonic chip is shown in Fig. 1(b).

* Corresponding authors.
E-mail addresses: ruili@dlut.edu.cn (R. Li), yewangsu@imech.ac.cn (Y. Su).

http://dx.doi.org/10.1016/j.ijsolstr.2016.12.006
0020-7683/

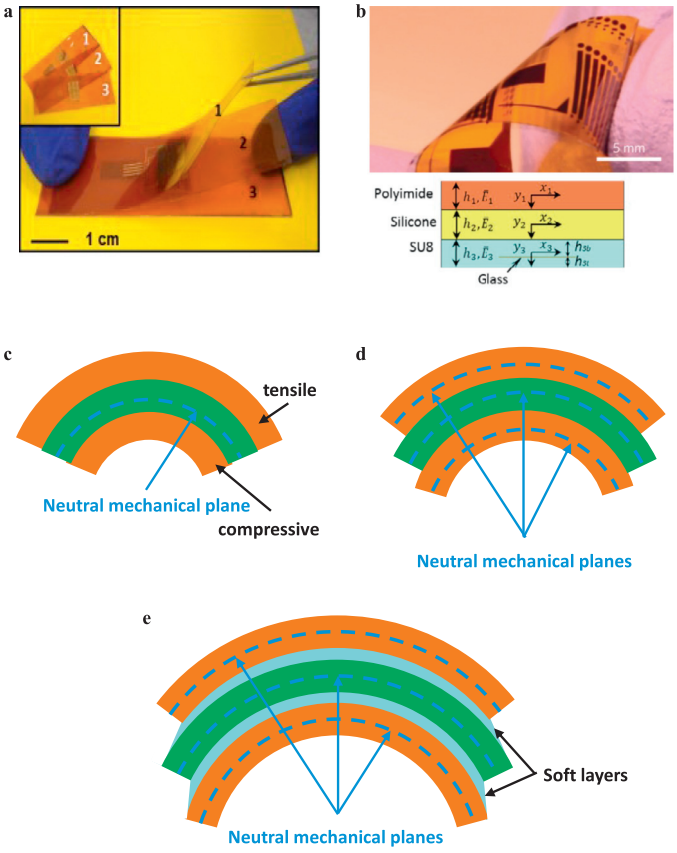

Fig. 1. (a) Stacking of three thin PZT-based piezoelectric layers. **(b)** A flexible photonic chip showing a linear array of microdisk resonators. **(c)** Perfect adhesion of three hard layers, with one neutral mechanical plane. **(d)** Ideal design: frictionless adhesion of the hard layers. **(e)** Splitting of the neutral mechanical plane by using the soft adhesive layers between the hard layers.

There is a critical mechanics issue in the design of a laminated structure of flexible electronics, i.e., how to stack the hard layers, where the brittle component is placed, in order that the entire electronic device exhibits the best performance while premature mechanical failure is avoided in repeated bending in use. Perfect adhesion of the hard layers seems to be the simplest design. However, as shown in Fig. 1(c), only one neutral mechanical plane exists in this case and the top and bottom layers will fail earlier, which can be easily captured by the classical beam theory (Timoshenko, 1930). Obviously, this design is less effective. An ideal design is that the hard layers adhere to each other without friction such that the layers bend independently and archive the strength of each simultaneously, as shown in Fig. 1(d), where each layer has its own neutral mechanical plane along its central axis. However, this design is not achievable in practice. Recently, splitting of the neutral mechanical plane has been proposed (Lu and Yang, 2015) and further applied (Li et al., 2016; Su et al., 2015b). It is also known as the local-neutral-axis design (Li et al., 2014) and is probably the best approach to the optimal and practical design. The basic idea is to split the neutral mechanical plane into each functional hard layer by using the soft adhesive layers between them, as shown in Fig. 1(e). In this way, the hard layers bend in almost the same mode, and archive the strength of each almost simultaneously. Since the soft adhesive layers play an important role in the realization of splitting of the neutral mechanical plane, to achieve the optimal design of a flexible electronics, quantitative investigation of the mechanical behavior of the laminated structure, including the soft adhesive layers, is necessary. Actually, there have been some recently published literatures developing the mechanics models for such laminated structures (Li et al., 2014; Li et al., 2016; Lu et al., 2014; Shi et al., 2014; Su et al., 2015b). However, previous studies fall into two categories: those simply taking into account the normal strain-induced deformation and neglecting the shear deformation of the soft adhesive layers (Li et al., 2014; Lu et al., 2014; Shi et al., 2014), and those incorporating the shear deformation of the soft adhesive layers (Li et al., 2016; Su et al., 2015b). It seems that the two categories would not yield big difference, but one will see in the following that this is not true. Actually, the importance of shear contribution in electronic devices based on polymeric flexible materials has been confirmed, which was used for understanding the shear piezoelectricity (Persano et al., 2016). For the laminated structure of flexible electronics, however, a problem of extreme importance arises: should the shear deformation be neglected in the soft adhesive layers?

This paper aims to quantitatively reveal a significant finding that shear deformation dominates in the soft adhesive layers of the laminated structure of flexible electronics while the normal strain-induced deformation is negligible by establishing an accurate enough analytic model of the structure. Since bending is the main mechanical behavior of the structure, we establish the analytic plane strain model under two representative bending loads, one with given slopes imposed at the ends of the hard layers and another with given slopes imposed at the end sections of the entire three-layer laminated structure. The effects of the membrane energy, bending energy and shear energy of the soft layer are investigated. Both the analytic model and the finite element analysis (FEA) validate the above finding. The developed model accurately predicts the strain distribution in each layer and the locations of the neutral mechanical planes of the top and bottom layers, thus they can provide design guidelines for the laminated structure-based flexible electronics.

2. Analytic model of the laminated structure

2.1. Given slopes are imposed at the ends of the hard layers

A three-layer laminated structure with length $2L$, thicknesses h_t, h_m and h_b for the top, middle and bottom layers is shown in Fig. 2(a), where the origin of the coordinate system xoy is located at the center of the top surface. The structure is bent by given slopes denoted by θ which are imposed at the ends of both the hard layers. Young's moduli and Poisson's ratios for the three layers are E_t, E_m and E_b, and ν_t, ν_m and ν_b, respectively. Due to the fact that the structure for flexible electronics is long and thin (Jia et al., 2011; Lee and Liu, 2014; Lin and Jain, 2009; Yu et al., 2013), the top and bottom layers behave as the slender beams and the model is known as the Euler–Bernoulli beam (Timoshenko, 1930). The soft middle layer is modeled as the shear lag which only accounts for the shear deformation; its validity will be discussed later. The right half structure is examined in the following due to the symmetry of both the structure and load conditions.

Thickness change of the structure is neglected since it is thin enough. The displacement at the central axes of the top and bottom layers are denoted by u_t and u_b, while the vertical displacement is denoted by v. The continuity yields the displacements of the top and bottom surfaces of the middle layer, denoted by u_m^t and u_m^b,

$$u_m^t = u_t - \frac{dv}{dx}\frac{h_t}{2},$$
$$u_m^b = u_b + \frac{dv}{dx}\frac{h_b}{2}. \quad (1)$$

According to Fig. 2(b), the shear strain of the middle layer, γ_m, is obtained. The membrane strains of the top and bottom layers, ε_t

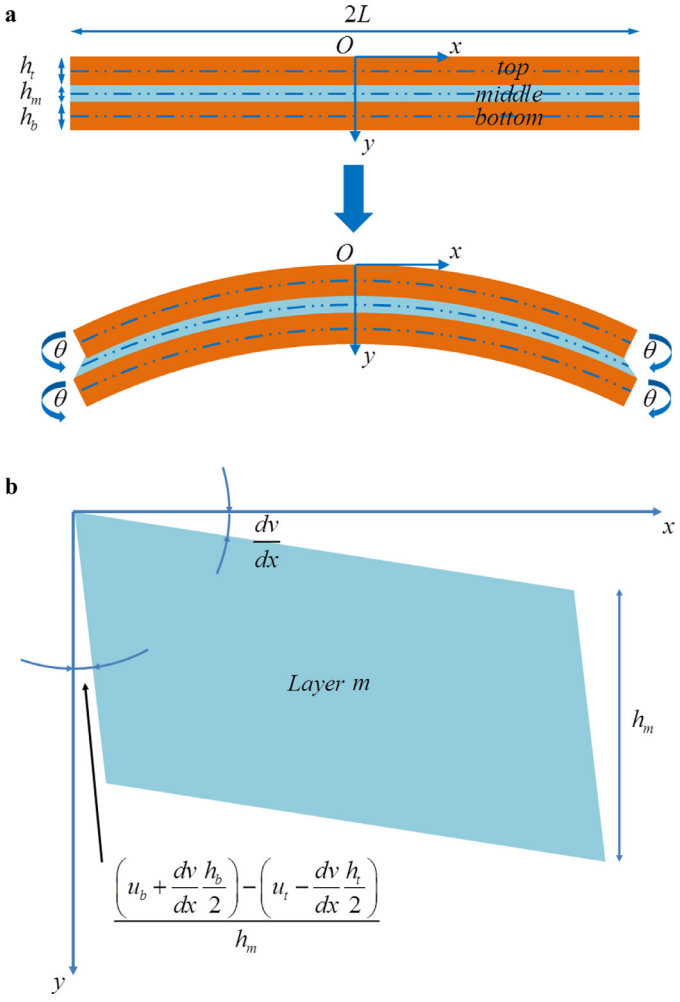

Fig. 2. Theoretical model of a three-layer laminated structure with given slopes imposed at the ends of the hard layers. **(a)** The stress-free and deformed states. **(b)** Shear strain of the middle layer.

and ε_b, and γ_m are

$$\varepsilon_t = \frac{du_t}{dx},$$
$$\varepsilon_b = \frac{du_b}{dx},$$
$$\gamma_m = \frac{dv}{dx} + \frac{u_m^b - u_m^t}{h_m} = \frac{dv}{dx} + \frac{1}{h_m}\left[u_b - u_t + \frac{1}{2}\frac{dv}{dx}(h_b + h_t)\right]. \quad (2)$$

The bending curvature of the structure, κ, is

$$\kappa = \frac{d^2v}{dx^2}. \quad (3)$$

The total elastic energy of the structure, U, includes the membrane energy and bending energy of the top and bottom layers as well as the shear energy of the middle layer. It is expressed as

$$U = \int_0^L \left(\frac{1}{2}\overline{EI}_b\kappa^2 + \frac{1}{2}\overline{EA}_b{\varepsilon_b}^2\right)dx + \int_0^L \left(\frac{1}{2}\overline{EI}_t\kappa^2 + \frac{1}{2}\overline{EA}_t{\varepsilon_t}^2\right)dx + \int_0^L \frac{1}{2}Gh_m{\gamma_m}^2dx, \quad (4)$$

where $\overline{EI}_t = E_t{h_t}^3/[12(1-{\nu_t}^2)]$ and $\overline{EA}_t = E_t h_t/(1-{\nu_t}^2)$, and $\overline{EI}_b = E_b{h_b}^3/[12(1-{\nu_b}^2)]$ and $\overline{EA}_b = E_b h_b/(1-{\nu_b}^2)$ are the effective bending stiffnesses and tensile stiffnesses of the top and bottom layers, respectively (Almeida and Ferreira, 1998); $G = E_m/[2(1+\nu_m)]$ is the shear modulus of the middle layer.

Substituting Eq. (2) into Eq. (4) gives the total energy. From the energy variation equation (Ekeland, 1974; Seliger and Whitham, 1968), $\delta U = 0$, we obtain the governing equations in terms of the displacements

$$\frac{d^4v}{dx^4} - \frac{Gh_m}{\overline{EI}_b + \overline{EI}_t}\left(\frac{h_b + h_t + 2h_m}{2h_m}\right)^2\frac{d^2v}{dx^2} - \frac{G}{\overline{EI}_b + \overline{EI}_t}\frac{h_b + h_t + 2h_m}{2h_m}\frac{d}{dx}(u_b - u_t) = 0,$$
$$\frac{d^2u_b}{dx^2} - \frac{G}{\overline{EA}_b}\frac{h_b + h_t + 2h_m}{2h_m}\frac{dv}{dx} - \frac{G}{\overline{EA}_b h_m}(u_b - u_t) = 0,$$
$$\frac{d^2u_t}{dx^2} + \frac{G}{\overline{EA}_t}\frac{h_b + h_t + 2h_m}{2h_m}\frac{dv}{dx} + \frac{G}{\overline{EA}_t h_m}(u_b - u_t) = 0, \quad (5)$$

and associated boundary conditions

$$u_t(0) = 0, u_b(0) = 0, v(0) = 0, v'(0) = 0, \frac{d^3v(0)}{dx^3} = 0,$$
$$u'_t(L) = 0, u'_b(L) = 0, v'(L) = \theta. \quad (6)$$

Eqs. (5) and (6) are rewritten as

$$\frac{d^4v}{dx^4} - a\frac{d^2v}{dx^2} - b\frac{d\Delta u}{dx} = 0,$$
$$\frac{d^2\Delta u}{dx^2} - \frac{ac}{b}\frac{dv}{dx} - c\Delta u = 0, \quad (7)$$

and

$$\Delta u(0) = 0, v(0) = 0, v'(0) = 0, \frac{d^3v(0)}{dx^3} = 0,$$
$$\Delta u'(L) = 0, v'(L) = \theta, \quad (8)$$

where $\Delta u = u_b - u_t$, $a = G(h_b + h_t + 2h_m)^2/[4h_m(\overline{EI}_b + \overline{EI}_t)]$, $b = G(h_b + h_t + 2h_m)/[2h_m(\overline{EI}_b + \overline{EI}_t)]$, and $c = G(1/\overline{EA}_b + 1/\overline{EA}_t)/h_m$.

The solution of Eq. (7) is

$$v = \frac{cp^2\cosh(pL)x^2 + 2a[\cosh(px) - 1]}{2Lcp^2\cosh(pL) + 2ap\sinh(pL)}\theta,$$
$$\Delta u = -\frac{\theta ac[p\cosh(pL)x - \sinh(px)]}{b[Lcp\cosh(pL) + a\sinh(pL)]}, \quad (9)$$

where $p = \sqrt{a+c}$. In combination with Eq. (5), we have

$$u_t = -\frac{\overline{EA}_b}{\overline{EA}_b + \overline{EA}_t}\Delta u = \frac{\overline{EA}_b}{\overline{EA}_b + \overline{EA}_t}\frac{\theta ac[p\cosh(pL)x - \sinh(px)]}{b[Lcp\cosh(pL) + a\sinh(pL)]},$$
$$u_b = \frac{\overline{EA}_t}{\overline{EA}_b + \overline{EA}_t}\Delta u = -\frac{\overline{EA}_t}{\overline{EA}_b + \overline{EA}_t}\frac{\theta ac[p\cosh(pL)x - \sinh(px)]}{b[Lcp\cosh(pL) + a\sinh(pL)]}. \quad (10)$$

The membrane strains of the top and bottom layers, the shear strain of the middle layer and the bending curvature of the structure are

$$\varepsilon_t = \frac{du_t}{dx} = \frac{\overline{EA}_b}{\overline{EA}_b + \overline{EA}_t}\frac{\theta acp[\cosh(pL) - \cosh(px)]}{b[Lcp\cosh(pL) + a\sinh(pL)]},$$
$$\varepsilon_b = \frac{du_b}{dx} = -\frac{\overline{EA}_t}{\overline{EA}_b + \overline{EA}_t}\frac{\theta acp[\cosh(pL) - \cosh(px)]}{b[Lcp\cosh(pL) + a\sinh(pL)]},$$
$$\gamma_m = \frac{dv}{dx} + \frac{1}{h_m}\left[\Delta u + \frac{1}{2}\frac{dv}{dx}(h_b + h_t)\right] = \frac{\theta a\left(c\frac{1}{h_m} + b\frac{h_b + h_t + 2h_m}{2h_m}\right)\sinh(px)}{b[Lcp\cosh(pL) + a\sinh(pL)]}, \quad (11)$$

and

$$\kappa = \frac{d^2v}{dx^2} = \frac{\theta p[c\cosh(pL) + a\cosh(px)]}{Lcp\cosh(pL) + a\sinh(pL)}. \quad (12)$$

The axial strain distribution in the top and bottom layers is (Timoshenko, 1953)

$$\varepsilon = \begin{cases} \varepsilon_t - \kappa\left(y - \frac{h_t}{2}\right) & \text{for } 0 \le y \le h_t, \\ \varepsilon_b - \kappa\left(y - h_t - h_m - \frac{h_b}{2}\right) & \text{for } h_t + h_m \le y \le h_t + h_m + h_b. \end{cases} \tag{13}$$

By equating ε in Eq. (13) to zero, the locations of the neutral mechanical planes of the top and bottom layers can be pinpointed:

$$y_t = \frac{\varepsilon_t}{\kappa} + \frac{h_t}{2}, \qquad y_b = \frac{\varepsilon_b}{\kappa} + h_t + h_m + \frac{h_b}{2}, \tag{14}$$

where y_t and y_b are respectively the distances along the thickness direction from the top surface of the laminate to the neutral mechanical planes of the top and bottom layers.

For convenience, we focus on a simplified case where $E_t = E_b = E$, $h_t = h_b = h$ and $\nu_t = \nu_b = \nu_m = \nu$. The membrane strains of the top and bottom layers, the shear strain of the middle layer and the bending curvature of the structure are obtained as

$$\varepsilon_t = \frac{1}{2}\frac{\theta q\left(1+\bar{h}_m\right)\sqrt{4/\bar{h}_m+6+3\bar{h}_m}\left[\cosh\left(q\sqrt{4/\bar{h}_m+6+3\bar{h}_m}\rho\right)-\cosh\left(q\sqrt{4/\bar{h}_m+6+3\bar{h}_m}\rho\bar{x}\right)\right]}{\rho q\sqrt{4/\bar{h}_m+6+3\bar{h}_m}\cosh\left(q\sqrt{4/\bar{h}_m+6+3\bar{h}_m}\rho\right)+3\left(1+\bar{h}_m\right)^2\sinh\left(q\sqrt{4/\bar{h}_m+6+3\bar{h}_m}\rho\right)},$$

$$\varepsilon_b = -\frac{1}{2}\frac{\theta q\left(1+\bar{h}_m\right)\sqrt{4/\bar{h}_m+6+3\bar{h}_m}\left[\cosh\left(q\sqrt{4/\bar{h}_m+6+3\bar{h}_m}\rho\right)-\cosh\left(q\sqrt{4/\bar{h}_m+6+3\bar{h}_m}\rho\bar{x}\right)\right]}{\rho q\sqrt{4/\bar{h}_m+6+3\bar{h}_m}\cosh\left(q\sqrt{4/\bar{h}_m+6+3\bar{h}_m}\rho\right)+3\left(1+\bar{h}_m\right)^2\sinh\left(q\sqrt{4/\bar{h}_m+6+3\bar{h}_m}\rho\right)},$$

$$\gamma_m = \frac{\theta\left(1/\bar{h}_m+1\right)\left[1+3\left(1+\bar{h}_m\right)^2\right]\sinh\left(q\sqrt{4/\bar{h}_m+6+3\bar{h}_m}\rho\bar{x}\right)}{\rho q\sqrt{4/\bar{h}_m+6+3\bar{h}_m}\cosh\left(q\sqrt{4/\bar{h}_m+6+3\bar{h}_m}\rho\right)+3\left(1+\bar{h}_m\right)^2\sinh\left(q\sqrt{4/\bar{h}_m+6+3\bar{h}_m}\rho\right)}, \tag{15}$$

and

$$\kappa = \frac{\theta\sqrt{4/\bar{h}_m+6+3\bar{h}_m}\left[\cosh\left(q\sqrt{4/\bar{h}_m+6+3\bar{h}_m}\rho\right)+3\left(1+\bar{h}_m\right)^2\cosh\left(q\sqrt{4/\bar{h}_m+6+3\bar{h}_m}\rho\bar{x}\right)\right]}{\rho h\sqrt{4/\bar{h}_m+6+3\bar{h}_m}\cosh\left(q\sqrt{4/\bar{h}_m+6+3\bar{h}_m}\rho\right)+3h\left(1+\bar{h}_m\right)^2/q\sinh\left(q\sqrt{4/\bar{h}_m+6+3\bar{h}_m}\rho\right)}. \tag{16}$$

where $q = \sqrt{E_m(1-\nu)/E}$, $\bar{h}_m = h_m/h$, $\rho = L/h$ and $\bar{x} = x/L$. From Eqs. (14) and (15), the non-dimensional location coordinates of the neutral mechanical planes of the top and bottom layers are obtained as

$$\bar{y}_t = \frac{y_t}{h} = \frac{1}{2}\frac{\left(1+\bar{h}_m\right)\left[\cosh\left(q\sqrt{4/\bar{h}_m+6+3\bar{h}_m}\rho\right)-\cosh\left(q\sqrt{4/\bar{h}_m+6+3\bar{h}_m}\rho\bar{x}\right)\right]}{\cosh\left(q\sqrt{4/\bar{h}_m+6+3\bar{h}_m}\rho\right)+3\left(1+\bar{h}_m\right)^2\cosh\left(q\sqrt{4/\bar{h}_m+6+3\bar{h}_m}\rho\bar{x}\right)}+\frac{1}{2},$$

$$\bar{y}_b = \frac{y_b}{h} = -\frac{1}{2}\frac{\left(1+\bar{h}_m\right)\left[\cosh\left(q\sqrt{4/\bar{h}_m+6+3\bar{h}_m}\rho\right)-\cosh\left(q\sqrt{4/\bar{h}_m+6+3\bar{h}_m}\rho\bar{x}\right)\right]}{\cosh\left(q\sqrt{4/\bar{h}_m+6+3\bar{h}_m}\rho\right)+3\left(1+\bar{h}_m\right)^2\cosh\left(q\sqrt{4/\bar{h}_m+6+3\bar{h}_m}\rho\bar{x}\right)}+\left(\bar{h}_m+\frac{3}{2}\right). \tag{17}$$

It is seen that the locations of the neutral mechanical planes are independent of the applied slopes. The discussion of some extreme cases from Eq. (17) is helpful in the design of the laminated structure. **(i)** The middle layer is soft enough. In this case, $E_m \to 0$ and thus $q \to 0$ such that $\bar{y}_t \to \frac{1}{2}$ and $\bar{y}_b \to \bar{h}_m + \frac{3}{2}$, which implies that the top and bottom layers bend independently and each layer has its own neutral mechanical plane along its central axis. **(ii)** The middle layer is hard enough. In this case, $E_m \to \infty$ and thus $q \to \infty$ such that $\bar{y}_t \to \frac{1}{2}\bar{h}_m + 1$ and $\bar{y}_b \to \frac{1}{2}\bar{h}_m + 1$ except at $\bar{x} = 1$ where $\bar{y}_t \to \frac{1}{2}$ and $\bar{y}_b \to \bar{h}_m + \frac{3}{2}$ hold. This implies that there is only one neutral mechanical plane except at the end of the laminated structure where each layer has its own neutral mechanical plane along its central axis. **(iii)** The length of the structure is much smaller than its thickness. In this case, $\rho \to 0$ such that the result is the same as that in case (i). **(iv)** The length of the structure is much larger than its thickness. In this case, $\rho \to \infty$ such that the result is the same as that in case (ii). **(v)** The thickness of the middle layer is much smaller than that of the top and bottom layers. In this case, $h_m \to 0$ such that the result is the same as that in case (ii).

To quantitatively illustrate the effects of $\bar{h}_m$ and ρ on the distribution of the strains and the locations of the neutral mechanical planes, an example is given, in which $E = 1$ GPa, $E_m = 100$ kPa, $\nu = 0.4$ and $h = 10\mu$m. Take $\theta/\rho = 10^{-4}$; this implies that the slope per unit length of the top and bottom layers is kept constant. Fig. 3 plots the membrane strain distribution in both the top and bottom layers for $\bar{h}_m = 1$ and $\rho = 100,\ 200,\ 400,\ 1000$ (Fig. 3(a)), and for $\rho = 100$ and $\bar{h}_m = 0.5,\ 1,\ 2$ (Fig. 3(b)). The present analytic results are validated by the FEM via ABAQUS software package (see appendix for details of the FEA). It is seen from Fig. 3 that very good agreement is achieved. The membrane strains of the top and bottom layers increase with ρ and approach constants for relatively large ρ except around the end of the structure, as revealed in Fig. 3(a). On the other hand, the membrane strains decrease with $\bar{h}_m$, as revealed in Fig. 3(b). Therefore, short laminated structure and thick middle layer are beneficial for reduction of the membrane strains in the hard layers.

In Fig. 4, the shear strains of the middle layer are shown for $\bar{h}_m = 1$ and $\rho = 100,\ 200,\ 400,\ 1000$ (Fig. 4(a)), $\rho = 100$ and $\bar{h}_m = 0.5,\ 1,\ 2$ (Fig. 4(b)), and $\rho = 300$ and $\bar{h}_m = 0.5,\ 1,\ 2$

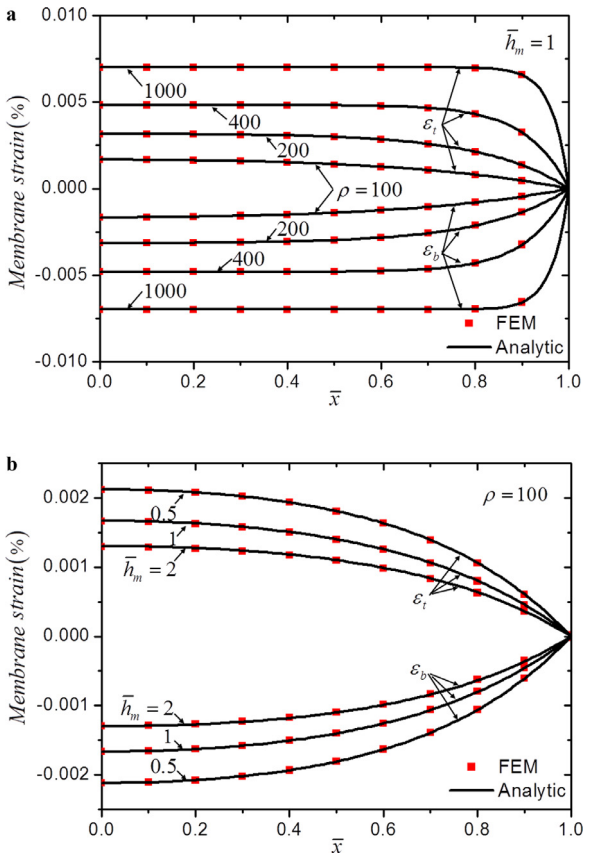

Fig. 3. Membrane strain distribution in both the top and bottom layers for **(a)** $\bar{h}_m = 1$ and **(b)** $\rho = 100$.

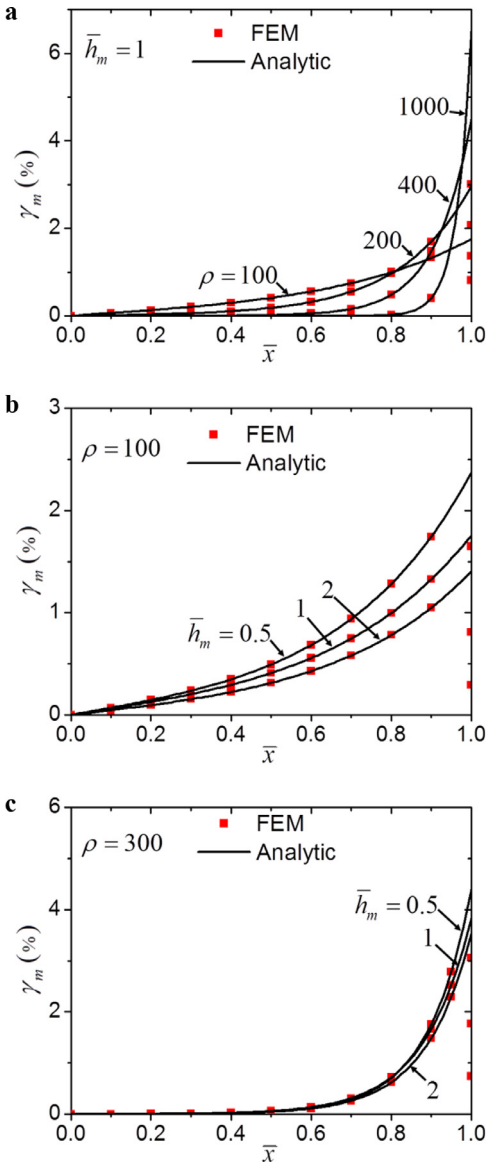

Fig. 4. Shear strain distribution in the middle layer for **(a)** $\bar{h}_m = 1$, **(b)** $\rho = 100$ and **(c)** $\rho = 300$.

(Fig. 4(c)), respectively. It is shown in Fig. 4(a) that the shear strain of the middle layer decreases with ρ around $\bar{x} = 0$ (the center of the structure) but increases with ρ around $\bar{x} = 1$ (the end of the structure). On the other hand, the shear strain decreases with $\bar{h}_m$ for relatively short structure (Fig. 4(b)). For relatively long structure (Fig. 4(c)), very small effect of $\bar{h}_m$ is detected on the shear strain which approaches zero except around the end of the structure where the shear strain decreases with $\bar{h}_m$.

Fig. 5 shows the non-dimensional location coordinates of the neutral mechanical planes of the top and bottom layers for $\bar{h}_m = 1$ (Fig. 5(a)) and $\rho = 100$ (Fig. 5(b)). It is concluded that the neutral mechanical planes shift toward the center of the hard layers with the decrease of ρ and the increase of $\bar{h}_m$; this means that short laminated structure and thick middle layer help to split the neutral mechanical plane into two lying in each hard layer where the brittle device is placed. In this way, the strength of each layer is reached almost simultaneously, which could avoid the premature failure of the entire device.

2.2. Given slopes are imposed at the end sections of the entire structure

To study the effects of the boundary conditions, another representative bending load is investigated. As shown in Fig. 6(a), the laminated structure is bent by given slopes θ which are imposed at the end sections of the entire structure. Compared with the model of Section 2, only the boundary conditions in Eq. (8) are changed to

$$\Delta u(0) = 0,\ v(0) = 0,\ v'(0) = 0,\ \frac{d^3 v(0)}{dx^3} = 0,$$
$$\gamma_m(L) = 0, v'(L) = \theta. \tag{18}$$

The solution of Eq. (7) becomes

$$v = \frac{1}{2}\frac{\theta}{L}x^2,\ \Delta u = -\frac{a\theta}{bL}x. \tag{19}$$

In combination with Eq. (5), we have

$$u_t = \frac{\overline{EA}_b}{\overline{EA}_b + \overline{EA}_t}\frac{a\theta}{bL}x,$$
$$u_b = -\frac{\overline{EA}_t}{\overline{EA}_b + \overline{EA}_t}\frac{a\theta}{bL}x. \tag{20}$$

Under the same simplified conditions with $E_t = E_b = E$, $h_t = h_b = h$ and $\nu_t = \nu_b = \nu_m = \nu$ as those in Section 2, the membrane strains of the top and bottom layers, the shear strain of the middle layer and the bending curvature of the structure are obtained as

$$\varepsilon_t = \frac{1}{2}\left(1 + \bar{h}_m\right)\frac{\theta}{\rho},\ \varepsilon_b = -\frac{1}{2}\left(1 + \bar{h}_m\right)\frac{\theta}{\rho},\ \gamma_m = 0, \tag{21}$$

and

$$\kappa = \frac{\theta}{\rho h}. \tag{22}$$

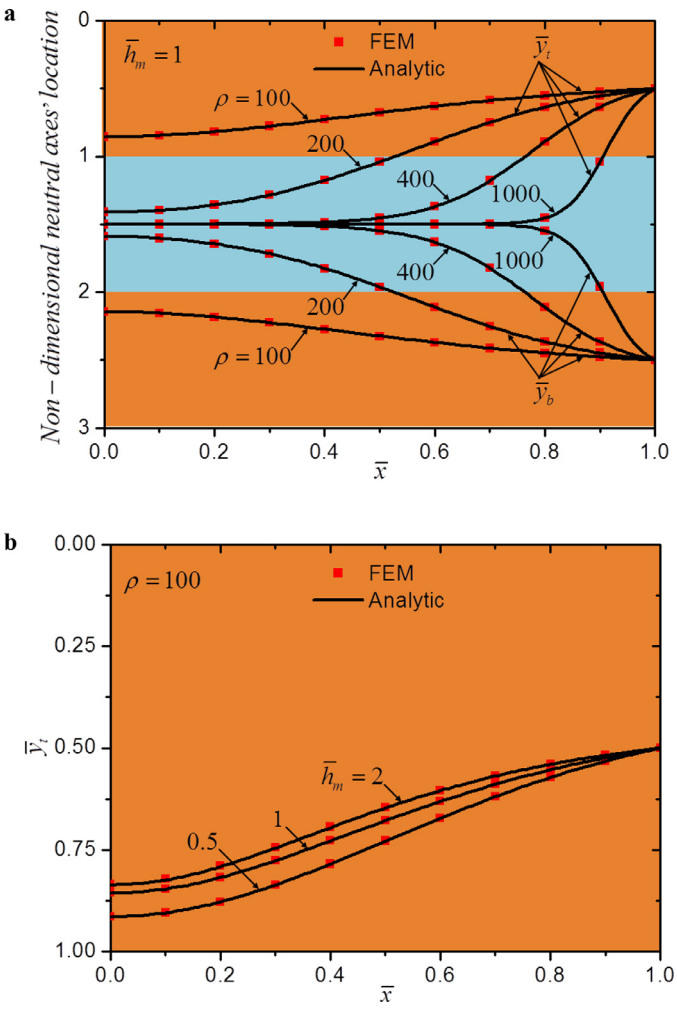

Fig. 5. Non-dimensional location coordinates of the neutral mechanical planes in **(a)** the top and bottom layers for $\bar{h}_m = 1$ and **(b)** the top layer for $\rho = 100$.

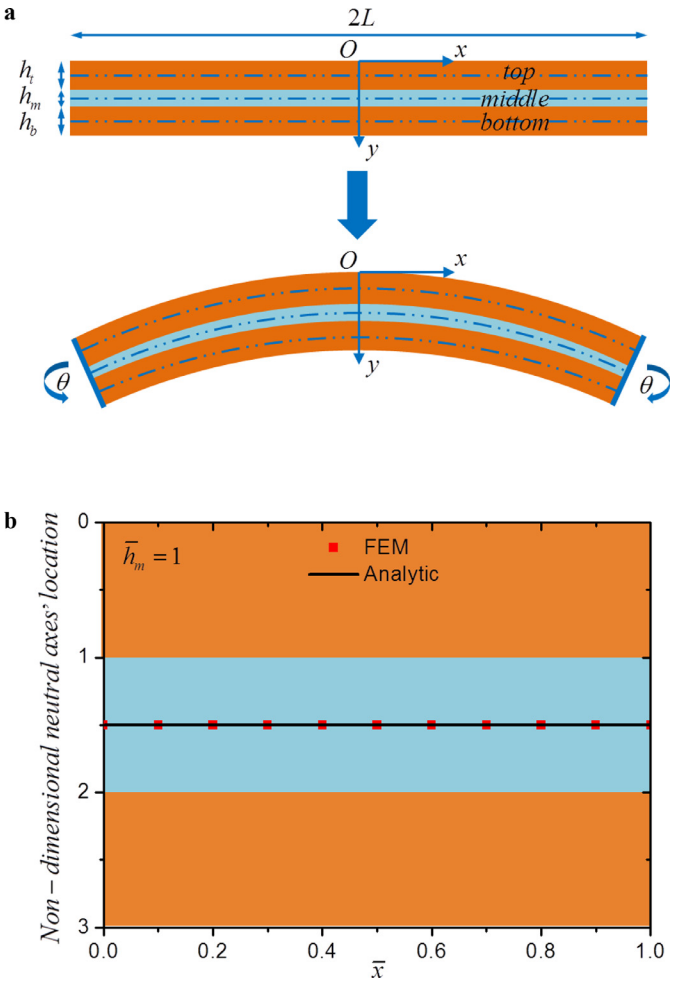

Fig. 6. **(a)** Theoretical model of a three-layer laminated structure with given slopes imposed at the end sections of the entire structure. **(b)** Non-dimensional location coordinates of the neutral mechanical plane of the structure.

The non-dimensional location coordinates of the neutral mechanical planes of the top and bottom layers are obtained as

$$\bar{y}_t = \bar{y}_b = 1 + \frac{\bar{h}_m}{2}. \tag{23}$$

This implies that there is only one neutral mechanical plane at the central plane of the structure, which corresponds to the pure bending. Fig. 6(b) shows the non-dimensional location coordinates of the neutral mechanical plane of the structure. From Sections 2 and 3, it is obvious that splitting of the neutral mechanical plane depends not only on the Young's moduli, thicknesses and length of the layers (Hohe et al., 2006; Kim et al., 2010; Li and Kardomateas, 2008; Rogers et al., 2010; Zhu et al., 2008), but also on the boundary conditions imposed.

3. Effects of the membrane energy and bending energy of the middle layer

In the above sections, only the shear energy is incorporated for the middle layer. Although the FEM results have validated the approximation, it is indispensable to investigate the effects of the membrane energy and bending energy. In the following, the laminated structure with given slopes imposed at the ends of the hard layers are considered, as illustrated in Section 2. Two models are examined, one fully incorporating the shear energy, membrane energy and bending energy and another neglecting the shear energy.

3.1. The model incorporating the shear energy, membrane energy and bending energy of the middle layer

In this model, the normal strain of the middle layer is regarded as the average of those at the top and bottom surfaces of the same layer. Therefore, the equivalent membrane strain ε_m and bending curvature κ_m of the middle layer are

$$\varepsilon_m = \frac{1}{2}\left(\varepsilon_t + \varepsilon_b + \frac{h_b - h_t}{2}\kappa\right),$$
$$\kappa_m = \frac{1}{h_m}\left(\varepsilon_t - \varepsilon_b - \frac{h_b + h_t}{2}\kappa\right). \tag{24}$$

The membrane energy and bending energy of the middle layer are integrated as

$$U' = \int_0^L \left[\frac{1}{2}\frac{\overline{EA}_m}{4}\left(\varepsilon_t + \varepsilon_b + \frac{h_b - h_t}{2}\kappa\right)^2 + \frac{1}{2}\frac{\overline{EI}_m}{{h_m}^2}\left(\varepsilon_b - \varepsilon_t + \frac{h_b + h_t}{2}\kappa\right)^2\right]dx, \tag{25}$$

where $\overline{EA}_m = E_m h_m/(1-{\nu_m}^2)$ and $\overline{EI}_m = E_m {h_m}^3/[12(1-{\nu_m}^2)]$ are the effective tensile stiffness and bending stiffness of the middle layer. In the following, these energies are not neglected for the middle layer.

Under the same simplified conditions with $E_t=E_b=E$, $h_t=h_b=h$ and $\nu_t=\nu_b=\nu_m=\nu$ as those in Section 2, the energy variation equation gives

$$\begin{aligned}
&\frac{d^4v}{dx^4}-\frac{G(h+h_m)^2/h_m}{2\overline{EI}+\overline{EI}_m h^2/h_m^2}\frac{d^2v}{dx^2}-\frac{G(h+h_m)/h_m}{2\overline{EI}+\overline{EI}_m h^2/h_m^2}\frac{d}{dx}(u_b-u_t)\\
&\quad+\underline{\frac{\overline{EI}_m h/h_m^2}{2\overline{EI}+\overline{EI}_m h^2/h_m^2}\frac{d^3}{dx^3}(u_b-u_t)}=0,\\
&\frac{d^2u_b}{dx^2}-\frac{G(h+h_m)/h_m}{\overline{EA}+\overline{EA}_m/4+\overline{EI}_m/h_m^2}\frac{dv}{dx}-\frac{G}{\left(\overline{EA}+\overline{EA}_m/4+\overline{EI}_m/h_m^2\right)h_m}\\
&\quad\times(u_b-u_t)+\underline{\frac{\overline{EA}_m/4-\overline{EI}_m/h_m^2}{\overline{EA}+\overline{EA}_m/4+\overline{EI}_m/h_m^2}\frac{d^2u_t}{dx^2}}\\
&\quad+\underline{\frac{\overline{EI}_m h/h_m^2}{\overline{EA}+\overline{EA}_m/4+\overline{EI}_m/h_m^2}\frac{d^3v}{dx^3}}=0,\\
&\frac{d^2u_t}{dx^2}+\frac{G(h+h_m)/h_m}{\overline{EA}+\overline{EA}_m/4+\overline{EI}_m/h_m^2}\frac{dv}{dx}+\frac{G}{\left(\overline{EA}+\overline{EA}_m/4+\overline{EI}_m/h_m^2\right)h_m}\\
&\quad\times(u_b-u_t)+\underline{\frac{\overline{EA}_m/4-\overline{EI}_m/h_m^2}{\overline{EA}+\overline{EA}_m/4+\overline{EI}_m/h_m^2}\frac{d^2u_b}{dx^2}}\\
&\quad-\underline{\frac{\overline{EI}_m h/h_m^2}{\overline{EA}+\overline{EA}_m/4+\overline{EI}_m/h_m^2}\frac{d^3v}{dx^3}}=0,
\end{aligned}\tag{26}$$

and

$$\begin{aligned}
&u_t(0)=0,\ u_b(0)=0, v(0)=0,\ v'(0)=0,\ \frac{d^3v(0)}{dx^3}=0,\\
&u'_t(L)=0,\ u'_b(L)=0,\ v'(L)=\theta,
\end{aligned}\tag{27}$$

where $\overline{EI}=Eh^3/[12(1-\nu^2)]$ and $\overline{EA}=Eh/(1-\nu^2)$. Eqs. (26) and (27) are simplified to

$$\begin{aligned}
&\frac{d^4v}{dx^4}-a'\frac{d^2v}{dx^2}-b'\frac{d\Delta u}{dx}+\underline{e\frac{d^3\Delta u}{dx^3}}=0,\\
&\frac{d^2\Delta u}{dx^2}-\frac{a'c'}{b'}\frac{dv}{dx}-c'\Delta u+\underline{\frac{a'c'e}{b'^2}\frac{d^3v}{dx^3}}=0,
\end{aligned}\tag{28}$$

and

$$\begin{aligned}
&\Delta u(0)=0,\ v(0)=0,\ v'(0)=0,\ \frac{d^3v(0)}{dx^3}=0,\\
&\Delta u'(L)=0,\ v'(L)=\theta,
\end{aligned}\tag{29}$$

where $a'=\frac{G(h+h_m)^2/h_m}{2\overline{EI}+\overline{EI}_m h^2/h_m^2}$, $b'=\frac{G(h+h_m)/h_m}{2\overline{EI}+\overline{EI}_m h^2/h_m^2}$, $c'=\frac{G}{(\overline{EA}/2+\overline{EI}_m/h_m^2)h_m}$, and $e=\frac{\overline{EI}_m h/h_m^2}{2\overline{EI}+\overline{EI}_m h^2/h_m^2}$. It is seen that Eqs. (26) and (28) have the same forms as Eqs. (5) and (7), respectively, except that there are the underlined terms appended. The solution of Eq. (28) under Eq. (29) is

$$\begin{aligned}
v&=\frac{c's^2\left(b'-a'e\right)\cosh(sL)x^2+2a'\left(b'-c'e\right)[\cosh(sx)-1]}{2Lc's^2(b'-a'e)\cosh(sL)+2a's(b'-c'e)\sinh(sL)}\theta,\\
\Delta u&=\frac{\theta a'c'\left(b'-a'e\right)}{Lb'c's(b'-a'e)\cosh(sL)+a'b'(b'-c'e)\sinh(sL)}\\
&\quad\times[\sinh(sx)-s\cosh(sL)x],
\end{aligned}\tag{30}$$

where

$$s=\frac{\sqrt{b'^2c'-2a'b'c'e+a'b'^2}}{\sqrt{b'^2-a'c'e^2}}.\tag{31}$$

u_t and u_b are

$$\begin{aligned}
u_t&=-\frac{1}{2}\Delta u\\
&=-\frac{1}{2}\frac{\theta a'c'\left(b'-a'e\right)}{Lb'c's(b'-a'e)\cosh(sL)+a'b'(b'-c'e)\sinh(sL)}\\
&\quad\times[\sinh(sx)-s\cosh(sL)x],\\
u_b&=\frac{1}{2}\Delta u\\
&=\frac{1}{2}\frac{\theta a'c'\left(b'-a'e\right)}{Lb'c's(b'-a'e)\cosh(sL)+a'b'(b'-c'e)\sinh(sL)}\\
&\quad\times[\sinh(sx)-s\cosh(sL)x].
\end{aligned}\tag{32}$$

Thus, we have

$$\begin{aligned}
\varepsilon_t&=-\frac{1}{2}\frac{\theta a'c'\left(b'-a'e\right)}{\rho hb'c's(b'-a'e)\cosh(s\rho h)+a'b'(b'-c'e)\sinh(s\rho h)}\\
&\quad\times[s\cosh(s\rho h\bar{x})-s\cosh(s\rho h)],\\
\varepsilon_b&=\frac{1}{2}\frac{\theta a'c'\left(b'-a'e\right)}{\rho hb'c's(b'-a'e)\cosh(s\rho h)+a'b'(b'-c'e)\sinh(s\rho h)}\\
&\quad\times[s\cosh(s\rho h\bar{x})-s\cosh(s\rho h)],\\
\gamma_m&=\frac{\theta a'\left(b'^2-a'c'e^2\right)s^2\sinh(s\rho h\bar{x})}{h\bar{h}_m\left[\rho hb'^2c's(b'-a'e)\cosh(s\rho h)+a'b'^2(b'-c'e)\sinh(s\rho h)\right]},
\end{aligned}\tag{33}$$

and

$$\kappa=\frac{c's\left(b'-a'e\right)\cosh(s\rho h)+a'\left(b'-c'e\right)s\cosh(s\rho h\bar{x})}{\rho hc's(b'-a'e)\cosh(s\rho h)+a'(b'-c'e)\sinh(s\rho h)}\theta.\tag{34}$$

The non-dimensional location coordinates of the neutral mechanical planes of the top and bottom layers are

$$\begin{aligned}
\bar{y}_t&=-\frac{1}{2}\frac{a'c'\left(b'-a'e\right)[s\cosh(s\rho h\bar{x})-s\cosh(s\rho h)]}{b'c's(b'-a'e)\cosh(s\rho h)+a'b'(b'-c'e)s\cosh(s\rho h\bar{x})}\\
&\quad+\frac{1}{2},\\
\bar{y}_b&=\frac{1}{2}\frac{a'c'\left(b'-a'e\right)[s\cosh(s\rho h\bar{x})-s\cosh(s\rho h)]}{b'c's(b'-a'e)\cosh(s\rho h)+a'b'(b'-c'e)s\cosh(s\rho h\bar{x})}\\
&\quad+\bar{h}_m+\frac{3}{2}.
\end{aligned}\tag{35}$$

3.2. The model neglecting the shear energy of the middle layer

In this model, the shear energy of the middle layer is neglected, thus Eq. (28) is simplified as

$$\begin{aligned}
&\frac{d^4v}{dx^4}+e\frac{d^3\Delta u}{dx^3}=0,\\
&\frac{d^2\Delta u}{dx^2}+\frac{a'c'e}{b'^2}\frac{d^3v}{dx^3}=0.
\end{aligned}\tag{36}$$

Eq. (29) still holds. The solution of Eq. (36) becomes

$$v=\frac{1}{2}\frac{\theta}{L}x^2,\quad \Delta u=0.\tag{37}$$

u_t and u_b are

$$u_t=0,\quad u_b=0.\tag{38}$$

Thus, we have

$$\varepsilon_t=0,\quad \varepsilon_b=0,\quad \gamma_m=\left(1+\frac{1}{\bar{h}_m}\right)\frac{\theta}{L}x,\tag{39}$$

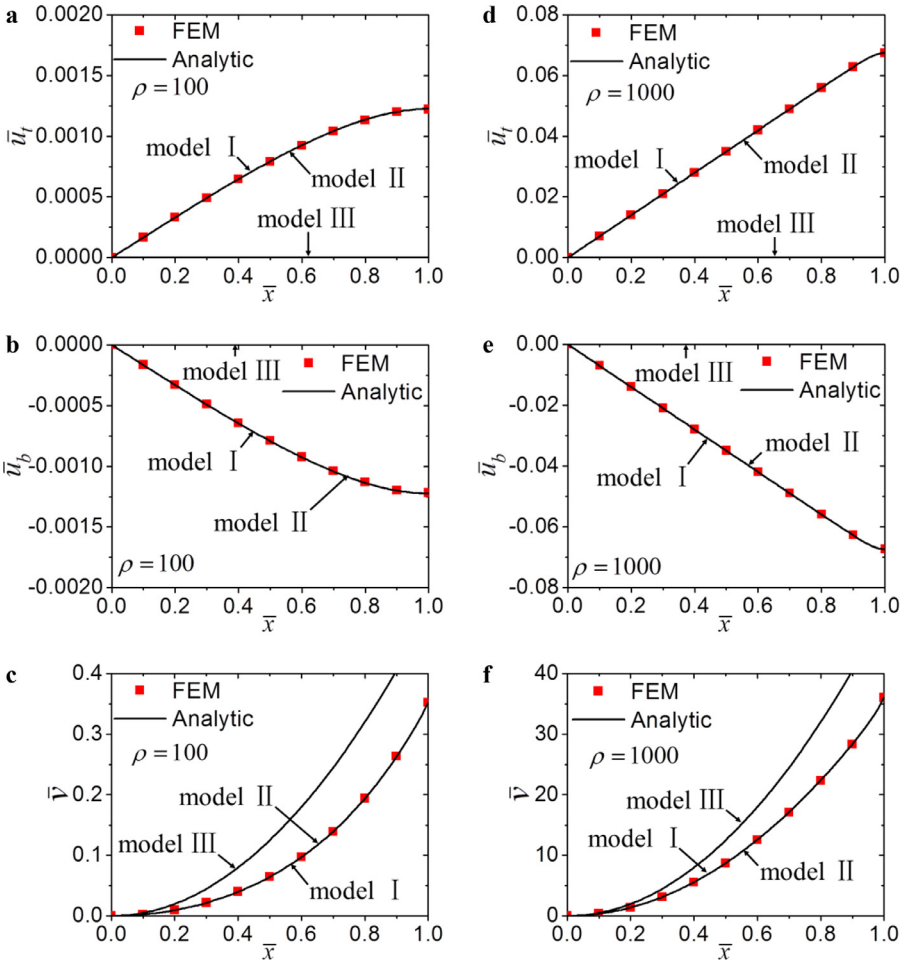

Fig. 7. Comparison of the displacements between the three models ($\bar{h}_m = 1$). Non-dimensional **(a)** axial displacements of the top layer, **(b)** axial displacements of the bottom layer and **(c)** transverse displacements of the structure for $\rho = 100$. Non-dimensional **(d)** axial displacements of the top layer, **(e)** axial displacements of the bottom layer and **(f)** transverse displacements of the structure for $\rho = 1000$.

and

$$\kappa = \frac{\theta}{L}. \tag{40}$$

The non-dimensional location coordinates of the neutral mechanical planes of the top and bottom layers are

$$\bar{y}_t = \frac{1}{2},\ \bar{y}_b = \frac{3}{2} + \bar{h}_m. \tag{41}$$

This implies that the top and bottom layers bend independently and each layer has its own neutral mechanical plane along its central axis.

To reveal the dominant mechanical behavior of the middle layer, comparison is made between the three models, i.e., the one only incorporating the shear energy (model I), the one fully incorporating the shear energy, membrane energy and bending energy (model II) and the one only neglecting the shear energy (model III). Fig. 7 shows the non-dimensional axial displacements of the top layer ($\bar{u}_t = u_t/h$) and bottom layer ($\bar{u}_b = u_b/h$) as well as transverse displacements of the structure ($\bar{v} = v/h$), where $\bar{h}_m = 1$, $\rho = 100$ (Fig. 7(a–c)) and 1000 (Fig. 7(d–f)). Fig. 8 shows the membrane strains of the top layer and shear strains of the middle layer for $\bar{h}_m = 1$ and $\rho = 100$ (Fig. 8(a,b)) and 1000 (Fig. 8(c,d)). The FEM results are also presented. It is obvious that model I agrees very well with model II and they both agree very well with FEM for every quantity, including both the displacements and strains, while model III yields large deviations from models I and II as well as FEM for all the results. This strongly supports the finding that the shear deformation dominates in the soft adhesive layer and the normal strain-induced deformation is negligible.

4. Conclusion

Laminated structure is used in flexible electronics to achieve both the excellent electric performance and attractive flexibility. An analytic mechanics model of the laminated structure is established in this paper to accurately predict the strain distribution of the structure and the locations of the neutral mechanical planes of the hard layers. By investigating the effects of the membrane energy and bending energy of a soft adhesive layer, it is found that shear deformation dominates in the soft layers of the laminated structure of flexible electronics. This FEM-validated finding solves a significant problem on whether the shear deformation should be neglected in the soft adhesive layers, which was not clarified in the previous studies. The developed model is very useful for the optimal design of the laminated structure-based flexible electronics.

Acknowledgements

Y.S. and R.L. acknowledge the support from the National Natural Science Foundation of China (grants 11572323 and 11302038). Y.S. also acknowledges the support from Chinese Academy of Sciences via the "Hundred Talent program" and the support from State Key

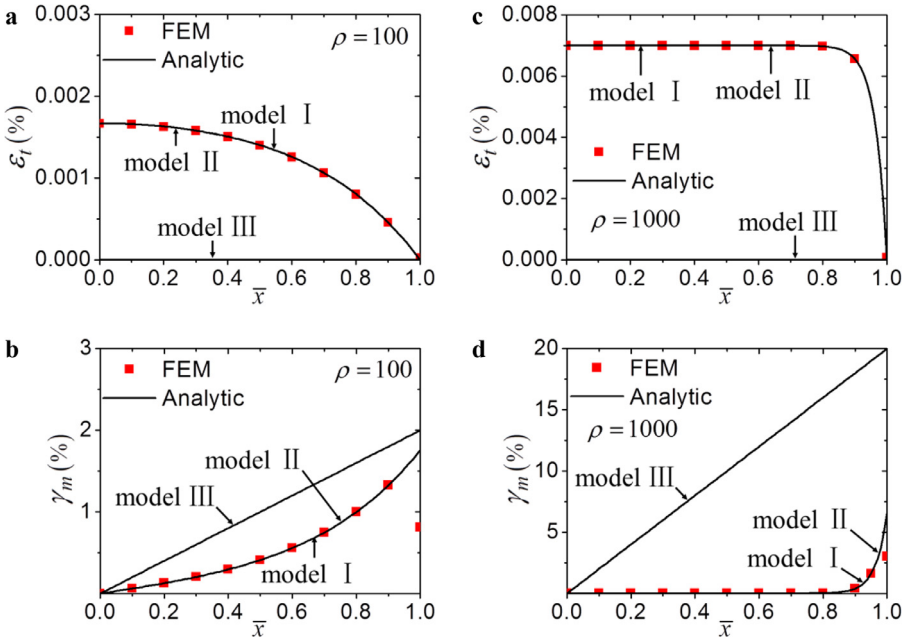

Fig. 8. Comparison of the strains between the three models ($\bar{h}_m = 1$). **(a)** Membrane strains of the top layer and **(b)** shear strains of the middle layer for $\rho = 100$. **(c)** Membrane strains of the top layer and **(d)** shear strains of the middle layer for $\rho = 1000$.

Laboratory of Structural Analysis for Industrial Equipment, Dalian University of Technology (No. GZ1603).

Appendix. Finite element analysis

FEA was conducted by using the ABAQUS software package to validate the analytic solutions of Eqs. (9), (10), (15), (17), (23), (32), (33), (37)–(39), as shown in Figs. 3–8. Due to the symmetry, only the right half of the three-layer laminated structure was analyzed. The left-hand side of the structure was clamped and the top and bottom layers were respectively attached to a rigid body at the right-hand side. To yield the plane strain state, the displacement along the width direction (z direction) was set to be zero. In-plane rotation with angle θ was imposed on the two rigid bodies to bend the structure. The 20-node quadratic brick element with reduced integration, C3D20R, was adopted for the three layers and the 4-node 3-D bilinear rigid quadrilateral element R3D4 for the rigid bodies. For the finite element meshes, the numbers of uniform grids for each layer are eight in the thickness direction (y direction) and one in the width direction. In the length direction (x direction), one grid was set at intervals of 1.25 h.

References

Allen, H.G., 1969. Analysis and Design of Structural Sandwich Panels, 1st ed. Pergamon Press, Oxford, New York.

Almeida, P.A.D., Ferreira, C.A.T., 1998. Determination of the effective bending stiffness of nailed laminated wood beams. In: 5th World Conference on Timber Engineering, 1, pp. 425–431. Proceedings.

Dagdeviren, C., Yang, B.D., Su, Y.W., Tran, P.L., Joe, P., Anderson, E., Xia, J., Doraiswamy, V., Dehdashti, B., Feng, X., Lu, B.W., Poston, R., Khalpey, Z., Ghaffari, R., Huang, Y.G., Slepian, M.J., Rogers, J.A., 2014. Conformal piezoelectric energy harvesting and storage from motions of the heart, lung, and diaphragm. Proc. Natl. Acad. Sci. USA 111, 1927–1932.

Ekeland, I., 1974. Variational principle. J. Math. Anal. Appl. 47, 324–353.

Hohe, J., Librescu, L., Oh, S.Y., 2006. Dynamic buckling of flat and curved sandwich panels with transversely compressible core. Compos. Struct. 74, 10–24.

Hwang, S.W., Tao, H., Kim, D.H., Cheng, H.Y., Song, J.K., Rill, E., Brenckle, M.A., Panilaitis, B., Won, S.M., Kim, Y.S., Song, Y.M., Yu, K.J., Ameen, A., Li, R., Su, Y.W., Yang, M.M., Kaplan, D.L., Zakin, M.R., Slepian, M.J., Huang, Y.G., Omenetto, F.G., Rogers, J.A., 2012. A physically transient form of silicon electronics. Science 337, 1640–1644.

Jia, Z., Tucker, M.B., Li, T., 2011. Failure mechanics of organic-inorganic multilayer permeation barriers in flexible electronics. Compos. Sci. Technol. 71, 365–372.

Kim, D.H., Ahn, J.H., Choi, W.M., Kim, H.S., Kim, T.H., Song, J.Z., Huang, Y.G.Y., Liu, Z.J., Lu, C., Rogers, J.A., 2008. Stretchable and foldable silicon integrated circuits. Science 320, 507–511.

Kim, D.H., Lu, N.S., Huang, Y.G., Rogers, J.A., 2012. Materials for stretchable electronics in bioinspired and biointegrated devices. MRS Bull 37, 226–235.

Kim, D.H., Lu, N.S., Ma, R., Kim, Y.S., Kim, R.H., Wang, S.D., Wu, J., Won, S.M., Tao, H., Islam, A., Yu, K.J., Kim, T.I., Chowdhury, R., Ying, M., Xu, L.Z., Li, M., Chung, H.J., Keum, H., McCormick, M., Liu, P., Zhang, Y.W., Omenetto, F.G., Huang, Y.G., Coleman, T., Rogers, J.A., 2011. Epidermal electronics. Science 333, 838–843.

Kim, D.H., Xiao, J.L., Song, J.Z., Huang, Y.G., Rogers, J.A., 2010. Stretchable, curvilinear electronics based on inorganic materials. Adv. Mater. 22, 2108–2124.

Ko, H.C., Stoykovich, M.P., Song, J.Z., Malyarchuk, V., Choi, W.M., Yu, C.J., Geddes, J.B., Xiao, J.L., Wang, S.D., Huang, Y.G., Rogers, J.A., 2008. A hemispherical electronic eye camera based on compressible silicon optoelectronics. Nature 454, 748–753.

Lee, Y.C., Liu, T.S., 2014. Deformation of multilayer flexible electronics subjected to Torque. Exp. Tech. 38, 13–20.

Li, L., Lin, H.T., Qiao, S.T., Zou, Y., Danto, S., Richardson, K., Musgraves, J.D., Lu, N.S., Hu, J.J., 2014. Integrated flexible chalcogenide glass photonic devices. Nat. Photonics 8, 643–649.

Li, R., Cheng, H.T., Su, Y.W., Hwang, S.W., Yin, L., Tao, H., Brenckle, M.A., Kim, D.H., Omenetto, F.G., Rogers, J.A., Huang, Y.G., 2013a. An analytical model of reactive diffusion for transient electronics. Adv. Funct. Mater. 23, 3106–3114.

Li, R., Li, M., Su, Y.W., Song, J.Z., Ni, X.Q., 2013b. An analytical mechanics model for the island-bridge structure of stretchable electronics. Soft. Matter. 9, 8476–8482.

Li, R.F., Kardomateas, G.A., 2008. Nonlinear high-order core theory for sandwich plates with orthotropic phases. AIAA J. 46, 2926–2934.

Li, S., Su, Y., Li, R., 2016. Splitting of the neutral mechanical plane depends on the length of the multi-layer structure of flexible electronics. Proc. R. Soc. A 472, 20160087.

Lin, K.L., Jain, K., 2009. Design and fabrication of stretchable multilayer self-aligned interconnects for flexible electronics and large-area sensor arrays using excimer laser photoablation. IEEE Electr. Device Lett. 30, 14–17.

Lu, N.S., Yang, S.X., 2015. Mechanics for stretchable sensors. Curr. Opin. Solid State Mater. Sci. 19, 149–159.

Lu, N.S., Yang, S.X., Qiao, S.T., 2014. Mechanics of flexible electronics and photonics based on inorganic micro-and nanomaterials. Proc SPIE 9083, 90831J.

Persano, L., Catellani, A., Dagdeviren, C., Ma, Y., Guo, X., Huang, Y., Calzolari, A., Pisignano, D., 2016. Shear piezoelectricity in Poly(vinylidenefl uoride-co-trifluoroethylene): full piezotensor coefficients by molecular modeling, biaxial transverse response, and use in suspended energy-harvesting nanostructures. Adv. Mater. 28, 7633–7639.

Rogers, J.A., Someya, T., Huang, Y.G., 2010. Materials and mechanics for stretchable electronics. Science 327, 1603–1607.

Seliger, R.L., Whitham, G.B., 1968. Variational principles in continuum mechanics. Proc. R. Soc. Lon. Ser.-A 305, 1-25.

Shi, Y., Rogers, J.A., Gao, C.F., Huang, Y.G., 2014. Multiple neutral axes in bending of a multiple-layer beam with extremely different elastic properties. J. Appl. Mech.-T. ASME 81, 114501.

Song, Y.M., Xie, Y.Z., Malyarchuk, V., Xiao, J.L., Jung, I., Choi, K.J., Liu, Z.J., Park, H., Lu, C.F., Kim, R.H., Li, R., Crozier, K.B., Huang, Y.G., Rogers, J.A., 2013. Digital cameras with designs inspired by the arthropod eye. Nature 497, 95–99.

Su, Y.W., Dagdeviren, C., Li, R., 2015a. Measured output voltages of piezoelectric devices depend on the resistance of voltmeter. Adv. Funct. Mater. 25, 5320–5325.

Su, Y.W., Li, R., Cheng, H.Y., Ying, M., Bonifas, A.P., Hwang, K.C., Rogers, J.A., Huang, Y.G., 2013. Mechanics of finger-tip electronics. J. Appl. Phys. 114, 164511.

Su, Y.W., Li, S.A., Li, R., Dagdeviren, C., 2015b. Splitting of neutral mechanical plane of conformal, multilayer piezoelectric mechanical energy harvester. Appl. Phys. Lett. 107, 041905.

Timoshenko, S., 1930. Strength of Materials. D. Van Nostrand company, inc., New York.

Timoshenko, S., 1953. History of strength of materials, with a brief account of the history of theory of elasticity and theory of structures. McGraw-Hill, New York,.

Xu, S., Zhang, Y.H., Cho, J., Lee, J., Huang, X., Jia, L., Fan, J.A., Su, Y.W., Su, J., Zhang, H.G., Cheng, H.Y., Lu, B.W., Yu, C.J., Chuang, C., Kim, T.I., Song, T., Shigeta, K., Kang, S., Dagdeviren, C., Petrov, I., Braun, P.V., Huang, Y.G., Paik, U., Rogers, J.A., 2013. Stretchable batteries with self-similar serpentine interconnects and integrated wireless recharging systems. Nat. Commun. 4, 1543.

Ying, M., Bonifas, A.P., Lu, N.S., Su, Y.W., Li, R., Cheng, H.Y., Ameen, A., Huang, Y.G., Rogers, J.A., 2012. Silicon nanomembranes for fingertip electronics. Nanotechnology 23, 344004.

Yu, S.H., Zhang, W.F., Li, L.X., Xu, D., Dong, H.L., Jin, Y.X., 2013. Transparent conductive Sb-doped SnO2/Ag multilayer films fabricated by magnetron sputtering for flexible electronics. Acta. Mater. 61, 5429–5436.

Zhu, F., Zhao, L.M., Lu, G.X., Wang, Z.H., 2008. Deformation and failure of blast-loaded metallic sandwich panels - Experimental investigations. Int. J. Impact Eng. 35, 937–951.